

Principles of Long Baseline Stellar Interferometry

Edited by Peter R. Lawson

Course Notes from the 1999 Michelson Summer School
August 15 –19, 1999

JPL Publication 00-009 07/00
<http://sim.jpl.nasa.gov/michelson/iss.html>

Contents

I	Introduction to Long-Baseline Stellar Interferometry	1
1	Why Build Stellar Interferometers?	3
	<i>by H.A. McAlister, Georgia State University</i>	
1.1	The Challenge	3
1.2	The Opportunity	5
1.3	Towards the Future	7
2	Elementary Theory of Interferometry	9
	<i>by A.F. Boden, California Institute of Technology</i>	
2.1	Introduction	9
2.2	A Simple Interferometer and a Monochromatic Source	10
2.3	Polychromatic Sources	12
2.4	Phase Reference of the Interferometer	15
2.5	Image Synthesis by Discrete Visibility Measurements	17
2.6	Visibilities of Various Flavors	18
2.7	Visibility of Common Source Morphologies	21
	2.7.1 Point Source	22
	2.7.2 Uniform Disk	23
	2.7.3 Multiple Stellar Systems	25
2.8	Summary	27
3	Beam Combination and Fringe Measurement	31
	<i>by W.A. Traub, Smithsonian Astrophysical Observatory</i>	
3.1	Elements of Beam Combination	32
	3.1.1 Single Aperture and Point Source	32
	3.1.2 Two Apertures and Point Source	38
	3.1.3 Two Apertures and Binary Star	40
	3.1.4 Two Apertures and Uniform Disk	40
	3.1.5 The Pocket Interferometer	41
	3.1.6 Two-Aperture Beam Pattern on Sky	42
	3.1.7 van Cittert–Zernike Theorem	43
3.2	Beam Combination in Practice	43
	3.2.1 Michelson’s Stellar Interferometer	43
	3.2.2 Image-Plane and Pupil-Plane Combination	45
	3.2.3 Beam splitter Phase-Shift	48
	3.2.4 Multiplexing Three or More Apertures	50
3.3	Visibility Loss Effects	51

3.3.1	Spectral Bandpass	52
3.3.2	Wavefront Tilt	52
3.3.3	Intensity Mismatch	53
3.3.4	Optical Surface Figure Errors	54
3.3.5	Polarization Effects	54
3.4	Visibility Enhancement Methods	55
3.4.1	Adaptive Optics	55
3.4.2	Fiber Optics	56
3.4.3	Integrated Optics	56
3.4.4	Nulling	56
4	Noise and Sensitivity in Interferometry	59
	<i>by C.H. Townes, University of California, Berkeley</i>	
4.1	Introduction	59
4.2	Wavefront Aberrations	59
4.3	Thermal and Quantum Noise	60
4.3.1	Noise Power Fluctuations	60
4.3.2	Signal-to-Noise Ratio	60
4.4	Heterodyne versus Direct-Detection Interferometry	61
4.4.1	Signal-to-Noise Ratio for Fringe Measurements	61
4.4.2	Bandwidth Considerations	62
4.4.3	Arrays with Multiple Telescopes	63
4.4.4	Coherence Time and Fringe Tracking	64
4.5	Conclusion	64
5	Observing Through the Turbulent Atmosphere	71
	<i>by A. Quirrenbach, University of California, San Diego</i>	
5.1	Introduction	71
5.2	The Kolmogorov Turbulence Model	72
5.2.1	Eddies in the Turbulent Atmosphere	72
5.2.2	The Structure Function for Kolmogorov Turbulence	72
5.2.3	Structure Function and Power Spectral Density of the Refractive Index	73
5.3	Wave Propagation Through Turbulence	74
5.3.1	The Effects of Turbulent Layers	74
5.3.2	Calculation of the Phase Structure Function	75
5.3.3	Phase-Coherence Function and Fried Parameter	76
5.4	The Effect of Turbulence on Images	76
5.4.1	Optical Image Formation	76
5.4.2	Diffraction-Limited Images and Seeing-Limited Images	77
5.4.3	The Significance of the Fried Parameter r_0	78
5.4.4	Strehl Ratio	79
5.4.5	Taylor Hypothesis and τ_0	80
5.4.6	Anisoplanatism	80

5.4.7	Scintillation	82
5.4.8	Turbulence and Wind Profiles	83
5.5	Appendix: Some Useful Facts from Fourier Theory	84
6	Design of Stellar Interferometers	87
	<i>by T.A. ten Brummelaar, Georgia State University</i>	
6.1	Introduction	87
6.2	What We Would Like to Measure	87
6.3	Logistics	88
6.4	Concrete and Steel	89
6.5	The Problem with the Atmosphere	90
6.6	Polarization	92
6.7	Internal Optical Quality	94
6.8	Diffraction	94
6.9	Dispersion	94
6.10	Controlling the Beast	95
6.11	Conclusion	96
II	Measurement and Calibration of Fringe Parameters	101
7	Visibility Estimation and Calibration	103
	<i>by M.M. Colavita, Jet Propulsion Laboratory</i>	
7.1	Introduction	103
7.2	Fringe Scanning and Matched Filtering	103
7.3	Visibility Estimation and Signal-to-Noise Ratio	104
7.4	Estimator Biases	106
7.5	Atmospheric Biases	108
	7.5.1 Spatial Wavefront Errors	108
	7.5.2 Temporal Errors	109
	7.5.3 Finite Coherence	109
	7.5.4 Mismatched Stroke	111
7.6	Conclusion	111
8	Phase and Group Delay Estimation	113
	<i>by P.R. Lawson, Jet Propulsion Laboratory</i>	
8.1	Motivation	114
8.2	Phase and Group Delay	115
8.3	Model of the Fringe	117
	8.3.1 Coherence Envelope	118
	8.3.2 Channeled Spectrum	119
8.4	Methods of Tracking Fringe Phase	123
	8.4.1 Phase Tracking with Four Quarter-Wavelength Steps	124
	8.4.2 Phase Tracking with a Linear Pathlength Sweep	125

8.4.3	Simultaneous Phase Measurements at Several Wavelengths	126
8.4.4	Triangle vs Sawtooth Modulations	127
8.5	Methods of Tracking Group-Delay	127
8.5.1	Channeled Spectrum: Fast Fourier Transform	129
8.5.2	Channeled Spectrum: Lomb-Scargle Periodogram	133
8.5.3	Channeled Spectrum: Least-Squares Fit	133
8.5.4	Multi-Wavelength Phasor Measurements: Fast or Direct Fourier Transform	134
8.5.5	Multi-Wavelength Phasor Measurements: “Optimal” Estimator	135
8.6	Variance of Phase and Group Delay Estimates	136
8.6.1	Variance of Phase	136
8.6.2	Variance of Group Delay	136
8.6.3	Phase and Group Delay Variance Compared	138
8.7	Conclusion	138
9	Phase Referencing	143
	<i>by A. Quirrenbach, University of California, San Diego</i>	
9.1	Introduction	143
9.2	Principles of Phase Referencing	144
9.2.1	The Mark III Interferometer	144
9.2.2	Visibility Estimation and Signal-to-Noise Ratio	146
9.2.3	Phase-Referenced Visibility Averaging	147
9.2.4	Limb Darkening of Arcturus	148
9.2.5	Further Applications of Same-Source Phase Referencing	149
9.2.6	Off-Source Phase Referencing	152
9.3	Phase Decorrelation Mechanisms	154
9.3.1	Phase Errors and Coherence Losses	154
9.3.2	Photon Noise in the Tracking Channel	154
9.3.3	Color and Visibility Dependence of the Effective Tracking Wavelength	155
9.3.4	Stroke Mismatch	155
9.3.5	Fringe Jumps	156
9.3.6	Dispersion	156
9.3.7	Anisoplanatism	157
9.3.8	Differential Refraction	157
9.3.9	Diffraction	160
III	Astrometry	163
10	Wide-Angle Astrometry	165
	<i>by D.J. Hutter, U.S. Naval Observatory</i>	
10.1	Introduction	165
10.2	Wide-Angle Astrometry	167

10.3	Baseline Metrology	167
10.4	Constant Term	168
10.5	Compensation of Atmospheric Effects	171
10.6	Current Status	172
11	Ground-Based Narrow-Angle Astrometry	177
	<i>by M.M. Colavita, Jet Propulsion Laboratory</i>	
11.1	Introduction	177
11.2	Atmospheric Effects	178
11.3	Other Errors	178
11.4	Implementing a Narrow-Angle Measurement	179
11.5	Conclusion	181
IV	Optical Synthesis Imaging	183
12	Interferometry with Two Telescopes	185
	<i>by H.M. Dyck, U.S. Naval Observatory</i>	
12.1	Introduction	185
12.2	Simple Concepts of Aperture Synthesis	185
12.3	Optical Delay and (u, v) Plane Tracks	189
12.4	Simple Models of Astrophysical Sources	190
	12.4.1 Binary Stars	192
	12.4.2 Stellar Angular Diameters	193
	12.4.3 Circumstellar Shells	194
12.5	Cautions and Caveats	196
12.6	Comparisons	196
13	An Introduction to Closure Phases	203
	<i>by J.D. Monnier, Smithsonian Astrophysical Observatory</i>	
13.1	Introduction	203
	13.1.1 Telescope Errors: Complex Gain	203
	13.1.2 Phase Referencing	206
13.2	The Closure Quantities	207
	13.2.1 Closure Phase and the Bispectrum	207
	13.2.2 Closure Amplitudes	208
	13.2.3 Measuring Closure Phases	209
	13.2.4 Closure Phase Relations	213
	13.2.5 Simple Cases	214
	13.2.6 Summary	216
13.3	Imaging	216
	13.3.1 Converting Bispectrum to Complex Visibilities	217
	13.3.2 Imaging Goals	218
	13.3.3 “Standard” Aperture Synthesis Imaging	219

13.3.4	Including Closure Phase Information	221
13.3.5	Imaging Results from Keck Aperture Masking	223
13.4	Outstanding Issues	224
13.4.1	Overview of Problems	224
13.4.2	New Possibilities	225
13.5	Summary of Important Points	226
14	Interferometer Design for Synthesis Imaging	231
	<i>by D. Mozurkewich, Naval Research Laboratory</i>	
14.1	Good Fringes vs Good Science	231
14.1.1	Alternative 1: Integrate Forever	234
14.1.2	Alternative 2: Sources with High Visibility	235
14.1.3	Alternative 3: Wavelength Bootstrapping	237
14.1.4	Alternative 4: Baseline Bootstrapping	239
14.1.5	Alternative 5: Guide Star Methods	240
14.2	Design of Interferometric Arrays	242
14.2.1	Optimal Design of Interferometric Arrays	242
14.2.2	Partially Redundant Arrays	242
14.2.3	Array Design with Vacuum Feed Systems	243
14.2.4	NPOI Configuration	243
14.2.5	Polarization and Beam Rotation	244
14.3	Beam Combination and Modulation	245
14.3.1	Pupil-Plane Combination: Passive Detection	245
14.3.2	Image-Plane Combination: Spatial Modulation	246
14.3.3	Pupil-Plane Combination: Temporal Modulation	247
14.3.4	Demodulating Multiple Baselines	248
14.4	Beam Combination Techniques	251
14.4.1	All-On-One Combination	251
14.4.2	Pairwise Combination	251
14.4.3	Partial Pairwise Combination	253
14.5	Comparison of Beam Combination Techniques	254
15	Data Reduction for Synthesis Imaging	257
	<i>by J.T. Armstrong, Naval Research Laboratory</i>	
15.1	Preliminaries	257
15.2	Planning the Observations	258
15.2.1	Stellar Diameters	259
15.2.2	Stellar Surface Structure	261
15.2.3	Binary-Star Separation	262
15.2.4	Circumstellar Material	263
15.3	Closure Phase and Calibration	263
15.4	Model Fitting and Imaging	265
15.5	Current Capabilities and Limitations	269

15.6	Future Developments	269
V	Nulling Interferometry	273
16	Nulling Interferometry and Planet Detection	275
	<i>by E. Serabyn, Jet Propulsion Laboratory</i>	
16.1	Introduction	275
16.2	Exozodiacal Light	276
16.3	Nulling Interferometry Basics	277
16.4	Symmetry and Stability Requirements	282
16.5	Rooftop-Based Rotational Shearing Interferometers	285
16.6	Experimental Results	287
16.7	Multi-Baseline Nulling	289
VI	Stellar Astronomy and Astrophysics	293
17	Binary Stars	295
	<i>by W.I. Hartkopf, U.S. Naval Observatory</i>	
17.1	Reason One: Binaries as Scales	296
	17.1.1 Part 1	296
	17.1.2 Part 2	296
17.2	Reason Two: Binaries as Yardsticks	301
17.3	Reason Three: Binaries and Stellar Evolution	301
17.4	Reason Four: Binaries in Other Guises	302
17.5	Reason Five: Binaries as “Vermin”	304
VII	Future Ground-Based Interferometry	309
18	Future Ground-Based Interferometry	311
	<i>by S.T. Ridgway, NOAO & Georgia State University</i>	
18.1	Existing Facilities and Scientific Output	311
18.2	Prospects for Astrophysics with Interferometers	313
18.3	Next Generation Ground-Based Array	315
	18.3.1 Near Infrared Capability	315
	18.3.2 Baseline of ~1000 m	315
	18.3.3 General Array Capabilities	315
	18.3.4 Number of Telescopes and Array Geometry	316
	18.3.5 Adaptive Optics and Aperture Size	317
	18.3.6 Budget Estimate	318
18.4	Astrophysical Potential of an IRVLA	318
18.5	Comments and Conclusion	320

Appendices	322
A Notes on the History of Stellar Interferometry	325
<i>by P.R. Lawson, Jet Propulsion Laboratory</i>	
A.1 Fizeau and Michelson	325
A.1.1 American References to European Work in Stellar Interferometry . .	326
A.1.2 Could Michelson Have Been Influenced by Fizeau Prior to 1890? . .	327
A.2 A Timeline of Stellar Interferometry: 1868–2000	329
B Suggested Reading	333
B.1 General References	333
B.2 Long Baseline Stellar Interferometers	335

Preface

Up until the latter half of the twentieth century, high angular resolution astronomy has been limited by the unsteadiness of images observed through the turbulent atmosphere. Although we are now able with adaptive optics to partially compensate for atmospheric seeing, even the largest telescopes are only able to resolve six or seven of the largest and nearest stars.

Further progress in high angular resolution astronomy can only be obtained through methods of interferometry. When the light from an *array* of telescopes is combined in an interferometer, the attainable resolution is limited not by the diameter of individual telescopes, but by the longest baseline spanning the array. Whereas interferometry has been well developed for use at radio wavelengths, with researchers involved both in national facilities and international collaborations, interferometry at optical and infrared wavelengths has yet remained relatively unexploited. Major new optical/infrared interferometers are now under construction by groups in both the United States and Europe and will soon open the field to new and exciting science. Longer-term plans are also underway by the National Aeronautics and Space Administration and the European Space Agency for the development of space-borne interferometers for astrometry, imaging, and planet detection. The technology for optical/infrared interferometry continues to develop rapidly, and exciting opportunities await astronomers and astrophysicists now entering this field.

Michelson Fellowship Program

The Michelson Fellowship Program, funded through NASA's Origins program and the Space Interferometry Mission, seeks to support the scientific community in building expertise in optical and infrared interferometry. The Michelson Fellowship Program brings together students and researchers in all stages of their career, through fellowships at the post-doctoral and graduate level, as well as through undergraduate research opportunities, and summer schools.

1999 Michelson Summer School

The 1999 Michelson Interferometry Summer School was held 9–13 August, 1999, at the California Institute of Technology in Pasadena, California. The school was attended by 43 graduate students, 13 post-doctoral level researchers, and 15 professional scientists. This was the first Summer School within the Michelson Fellowship Program and followed on from the Summer School on Optical/IR Interferometry hosted by the U.S. Naval Observatory in Flagstaff, Arizona, in October 1998. The lectures were given by staff of the Jet Propulsion Laboratory, the US Naval Observatory, the Naval Research Laboratory, and faculty and

staff from the University of California (at Berkeley and San Diego), Harvard University, and Georgia State University.

The lectures emphasized the fundamentals of astronomical interferometry, focusing principally on the engineering aspects of stellar interferometers. Subjects that were reviewed included the design of interferometric arrays, strategies for combining starlight, and the principles of observing, data reduction, modeling, and synthesis imaging.

The lectures were supplemented with day trips to the Mount Wilson Observatory and the Palomar Observatory. This provided the opportunity to visit the Infrared Spatial Interferometer, the CHARA Array, and the Palomar Testbed Interferometer, and the possibility for further discussions with the lecturers.

Overview of the Course Notes

These course notes document the lecture series from the 1999 Summer School. The lecture material was chosen to emphasize the development of ground-based interferometry and to include an introduction to the future possibilities of space missions within NASA's Origins Program. The material contained in the course notes is, however, primarily concerned with ground-based interferometry. Plans for space-based interferometry, although not described here, are well represented in the JPL publications describing the Space Interferometry Mission and the Terrestrial Planet Finder (see Appendix B).

Although most subjects are covered in detail in their respective chapters, certain subjects, such as the use of fiber optics, spatial filters, and adaptive optics, are mentioned only in passing. Some omissions were inevitable due to the limited scope of the Summer School, and so resources for further reading are included in the Appendices.

The course notes are divided into 7 parts and 18 chapters covering the major themes presented during the school. When reading from one chapter to another, please bear in mind that the notation is only consistent within individual chapters.

PETER R. LAWSON

Addendum

These course notes have been revised for re-issue on CDROM. The revision corrected minor errors in the text, updated the website addresses included in Chapter 1 and Appendix B, and improved the quality of the corresponding PDF files. I am most grateful to Chris Hawley at JPL for helping me resolve questions concerning L^AT_EX 2_ε, dvips, and PDF file conversion. This revision of the Course Notes in PDF format is also available at the Michelson Fellowship Program Website at <http://sim.jpl.nasa.gov/library/coursenotes.html>.

— PRL, December 6, 2000.

Acknowledgments

I would like to begin by thanking my wife Laurence for her patience and encouragement, my daughter Chloé for enduring a somewhat more hectic routine in August 1999, and my son Felix for staying where he was until after the dust settled—born August 30, 1999.

I offer my warmest thanks to the lecturers and authors who contributed to this volume. As a group they laughed at my early deadlines but were in time helpful, kind, and accommodating. I am grateful for their time and cooperation.

I would particularly like to thank Ken Johnston for his encouragement and for the financial support of staff from the U.S. Naval Observatory.

I was fortunate to have the advice of Mark Colavita, Mike Shao, and Steve Unwin in sorting out priorities, speakers, subjects, times, and overall content during the early stages of planning.

I take particular pleasure in thanking Jo Pitesky, Danika Jensen, and Debi Fambro, for helping bring the Summer School together. I am grateful to Jo and Danika for their efforts in shaping the Summer School, including (but not limited to) registration, accommodations, transportation, tours, lecture facilities, banquet arrangements, coffee breaks, video-taping, and audio-visual equipment. I am grateful to Debi for providing the travel arrangements for lecturers and students, and for her remarkable courtesy, efficiency, and patience.

For exceptional service through the JPL travel authorization office, I am most grateful to Laura Lee and Mariza Arnot.

My thanks also to Brian Knapp and Kalee Perrin for their efforts in the labour-intensive task of scanning viewgraphs into PDF format, and Arlene Dondoyano and Kate Weisberg at NASA Ames for copying the lectures onto real-video format.

The tours and facilities at the Mount Wilson Observatory were made possible through the Mount Wilson Institute with the generous help of Bob Jastrow, Mary Cragg, Sean Hoss, and the docents Mary Brown, Gale Gant, Don Nicholson, and Greg Smith. Access to and subsequent re-alignment of the CHARA Array was kindly provided by Hal McAlister, Theo ten Brummelaar, Steve Ridgway, Nils Turner, Laszlo Sturmman, and Joey Seymore. Access to the Infrared Spatial Interferometer was provided courtesy of C.H. Townes, Bill Danchi, John Monnier, and David Hale.

Facilities at the Palomar Observatory were made possible with the help of Wal Sargent, Bob Brucato, and Bob Thicksten. Tours of the Observatory and the Palomar Testbed

Interferometer were provided courtesy of staff at the Jet Propulsion Laboratory, including Andrew Booth, Andy Boden, Gerard van Belle, Kent Wallace, and Mark Colavita.

I would like to thank the Michelson Fellowship Program for its generous financial support for the editing of this volume. The Course Notes were edited with the assistance of Sunjay Moorthy, Mary Young, and Larry Palkovic at JPL Publications. The real or virtual book you hold was assembled using L^AT_EX 2_ε, and B^IB_TE_X with a standard `book` class modified to include PostScript fonts.

It is a great pleasure to thank Rudolf Danner and Mark Colavita for allowing what was previously only “a rewarding detour from my usual responsibilities” to become an integral part of my work at JPL.

The inside front cover photograph of Albert Michelson (standing in front of the Maryland Hotel) and inside back cover photograph of Francis Pease (using the 20-ft interferometer on the 100-in telescope) were provided courtesy of the Archives, California Institute of Technology.

The Michelson Fellowship Program is funded through NASA’s Origins program and the Space Interferometry Mission at the Jet Propulsion Laboratory. This work was carried out at the Jet Propulsion Laboratory, California Institute of Technology, under contract with the National Aeronautics and Space Administration.

PETER R. LAWSON
Jet Propulsion Laboratory
Pasadena, California
July 7, 2000

Part I

Introduction to Long-Baseline Stellar Interferometry

Chapter 1

Why Build Stellar Interferometers?

HAROLD A. MCALISTER

CENTER FOR HIGH ANGULAR RESOLUTION ASTRONOMY
GEORGIA STATE UNIVERSITY, ATLANTA, GEORGIA

1.1 The Challenge

Optical interferometers offer tremendous challenges and opportunities to suit the scientific tastes of those wishing to build instruments at the frontiers of technology that will enable science of an unprecedented nature. The minimum problem posed by interferometry is the combination at a beam splitter of light from a pair of telescopes whose baseline projected onto the sky determines the achievable resolution. In order to produce fringes at the beam splitter, one must match the paths followed by the two beams to a micron or so in length and hold them stable to a fraction of a wavelength of light. Herein lies the technical challenge. Numerous factors conspire to make the creation of fringes a devilishly difficult chore. Path delays and wavefront tilts are induced by the atmosphere even before light is collected by the telescopes, and then all the downstream subsystems further degrade the problem.

Thus, in order to produce fringes, interferometers are necessarily complex and nested systems possessing numerous sophisticated subsystems. The light collectors themselves, be they siderostats or telescopes, have complex controls and must be engineered to maintain stiffness and smoothness of operation. Their sheer numbers pose problems of maintenance that must not be underestimated. Optical delay lines are complex instruments occupying large physical spaces and are a primary facilities burden and cost driver for an interferometer. On the other hand, the technical basis for delay lines is quite mature and highly functional, and the devices work really very well. Beam combination schemes are an especially complicated issue, particularly when the number of collecting elements grows beyond

Table 1.1: Current Ground-Based Optical/Infrared Interferometers

Facility Acronym	Operating Institution(s)	Site Location	No. of Collecting Elements	Element Aperture (cm)	Maximum Baseline (m)	Operating Wavelength (microns)	Operating Status
GI2T	Obs. Côte d'Azur	Calern, FR	2	150	70	0.4–0.8 & >1.2	since 1985
ISI	UC Berkeley	Mt. Wilson, US	3	165	30+	10	since 1990
COAST	Cambridge U	Cambridge, UK	5	40	22	0.4–0.95 & 2.2	since 1991
SUSI	Sydney U	Narrabri, AU	13	14	640	0.4–0.66	since 1991
IOTA	CfA/U Mass	Mt. Hopkins, US	3	45	38	0.5–2.2	since 1993
NPOI	USNO/NRL	Anderson Mesa, US	6	60	435	0.45–0.85	since 1995
PTI	JPL/Caltech	Mt. Palomar, US	2	40	110	1.5–2.4	since 1995
MIRA-I	NAO Japan	Tokyo, Japan	2	25	4	0.8	since 1998
CHARA	Georgia St. U	Mt. Wilson, US	6	100	350	0.45–2.4	since 1999
KI	CARA	Mauna Kea, US	2(4)	1,000(180)	140	2.2–10	initial 2001
VLTI	ESO	Cerro Paranal, Chile	4(3)	820(180)	200	0.45–12	initial 2001
LBT	U Arizona, Italy, et al.	Mt. Graham, US	2	840	23	0.4–400	initial 2005?

half a dozen or so, and offer plenty of room for creative ingenuity. Alignment and stability offer interesting problems, and interferometers possess a depressingly large number of optical surfaces, each one of which represents loss of light and corruption of that which it passes downstream.

Many of these hardware subsystems have to be actively controlled and must work together with other subsystems. There is no shortage of really fascinating hardware to be designed, fabricated, installed, aligned, controlled and maintained in an interferometer. Thousands of lines of code must be written, tested and probably continuously debugged. Obviously, there is plenty of opportunity for failures along the way, but optimists would regard these risks part of the allure of interferometry.

In addition to the hardware/software issues, interferometers require new tools and algorithms for optimally scheduling observations and calibrating and archiving the data. Perhaps the most challenging problem in this area is the task of producing images of high fidelity and reliability.

Finally, there is the challenge of obtaining adequate funding to develop instruments in an area still regarded by most as developmental. In particular, one must avoid over-heightening expectations as to the kind of science forthcoming in the near term. To a considerable extent, speckle interferometry suffered in the 1970s and early 1980s from an exaggeration of its potential.

Many people find this sobering litany of problems to be the real meat of interferometry, and, rather than being discouraged, some very clever scientists and engineers have devoted much of their careers to solving the basic technical issues. Because of their efforts, we now have a modest retinue of interferometers around the world poised to provide a substantial body of science.

It has taken more than a century to extrapolate the basic physics of interferometry into the working (or nearly so) instruments listed in Tables 1.1 and 1.2. I include only ground-based

Table 1.2: Additional Information on Ground-Based Projects

Facility Acronym	Facility Name	Website (http://)
GI2T	Grand Interféromètre à 2 Télescopes	www.obs-nice.fr/fresnel/gi2t/en/
ISI	Infrared Spatial Interferometer	isi.ssl.berkeley.edu/
COAST	Cambridge Optical Aperture Synthesis Telescope	www.mrao.cam.ac.uk/telescopes/coast/
SUSI	Sydney University Stellar Interferometer	www.physics.usyd.edu.au/astron/astron.html
IOTA	Infrared/Optical Telescope Array	cfa-www.harvard.edu/cfa/oir/IOTA/
NPOI	Navy Prototype Optical Interferometer	ad.usno.navy.mil/npoi/
PTI	Palomar Testbed Interferometer	huey.jpl.nasa.gov/palomar/
MIRA-I	Mitaka optical-Infrared Array	tamago.mtk.nao.ac.jp/mira/
CHARA	Center for High Angular Resolution Astronomy (CHARA) Array	www.chara.gsu.edu/CHARA/
KI	Keck Interferometer	huey.jpl.nasa.gov/keck/
VLTi	Very Large Telescope Interferometer	www.eso.org/projects/vlti/
LBT	Large Binocular Telescope	medusa.as.arizona.edu/lbtwww/lbt.html

facilities in the tables (and in this discussion), but there is, of course, considerable activity and momentum in space-borne interferometers as well.

Current instruments explore four degrees of freedom (number and aperture of collecting elements, maximum baseline, and wavelength regime) with a level of incompleteness consistent with available funding. Each of these facilities has its own approach to solving the phasing problem, but all interferometers possess certain similarities. Some of these instruments are principally devoted to rather specific scientific problems such as absolute astrometry for NPOI and stellar diameters for SUSI. The reader can explore websites to see how each of these instruments has responded to the technical challenges of producing fringes.

Several of these instruments are lineal descendents of the Mark III interferometer that operated on Mount Wilson during the 1980s and presented solutions to most of the requisite technical challenges. The Mark III also produced important scientific results of high accuracy to lend confidence in the value of interferometry.

1.2 The Opportunity

What science can these instruments pursue? Will they live up to their promise? Will their scientific products engender the confidence of the scientific community to invest precious resources in next-generation instruments? Are we even building the right instruments now?

We can only hazard a guess at the first of these four questions. But it is a well-informed guess. Unquestionably, current interferometers possess wonderful resolution. The longest baseline facility now in existence is the Sydney University Stellar Interferometer (SUSI). Its limiting resolution of 100 micro-arcsec is a gain of four orders of magnitude over traditional ground-based direct imaging through photography and more than two orders of magnitude gain over adaptive optics corrected telescopes and over the Hubble Space Telescope. But SUSI and other long-baseline interferometers are extremely limited in sensitivity, and all interferometers inherently suffer from extremely narrow fields of view. A comparison with HST is thus a bit cavalier in terms of comparative sensitivity and field size.

The current generation of interferometers will primarily contribute to stellar astronomy. Their ability to play an important role in extragalactic astronomy (for example, through the direct imaging of broad-line regions of quasars) is made infeasible by their small apertures and/or relatively short baselines. Signal-to-noise ratio is a precious commodity to an interferometer where exposure times are limited by the atmospheric redistribution time t_0 , typically a few tens of milliseconds.

So, while interferometry will not soon satisfy the needs of the extragalactic community, the resolution and accuracy brought to bear on problems of stellar astrophysics will yield substantial new science. Fundamental new data for stars will be forthcoming in unprecedented quantity and quality. These data will include effective temperatures, surface fluxes, masses and luminosities for stars well distributed over spectral type and luminosity class. Sensitivity limitations will maintain the elusiveness of white dwarfs and the lower end of the main sequence, but, for the first time, tens of thousands of objects populating the majority of the H-R diagram will be accessible to high-resolution studies.

To be most useful, this flood of new data must be well calibrated. Measurements of the physical parameters for stars require accuracies at the couple of percent level in order to best challenge astrophysical theory. Resolution *and* accuracy are together the key to having the greatest scientific impact. Here, again, the history of speckle interferometry comes to mind in which casual calibration of potentially simple things like pixel scale led to results of little or no use even though significant amounts of large telescope time were consumed in their production.

We do not need thousands of new stellar masses accurate to 10%, but we do need hundreds accurate to 1%. Similarly, stellar limb darkening does not require confirmation but does need to be measured with sufficient accuracy to confront theory. Interferometrists need to establish more collaborations with theorists in selecting the optimal utilization of these wonderful new instruments.

In addition to the proliferation of basic data for stars, interferometers can and will contribute to a wide variety of problems. For single stars, such problems include the measurement of limb darkening, determination of linear diameters for stars with accurate parallaxes, studying phenomena associated with star formation (including dynamic phenomena) and pre-main sequence objects, measuring absolute rotation, stellar flares, p-mode oscillations and the pulsations of Cepheid and Mira variables (to include the direct geometric calibration of the period-luminosity relation for Cepheids), and phenomena associated with hot stars (shells, winds, etc.) and cool giants and supergiants. For binary stars, in addition to resolving the majority of the spectroscopic binaries and providing masses in large numbers, interferometric surveys for duplicity will be carried to new levels of completeness and close binary phenomena will be detected and maybe even imaged. Low mass companions, including those of planetary mass, may be astrometrically detected in binaries.

The first really interesting images from interferometry will involve the detection of surface features on normal stars and phenomena in the close-in environments of young stellar

objects. Interferometers will witness the eruptions of novae and perhaps even the explosion of a supernova.

We can predict, with great longing, many of the research enterprises to be opened by interferometry in the coming years. But we must keep in mind that we are dealing with multiple orders of magnitude increase in resolution. In a letter to the author in 1990, UCLA astronomer Daniel Popper remarked

History has taught us that whenever a new technique enters a new realm of observational phase space, the most striking and productive results tend to be those not anticipated by even the most prescient thinkers.

Professor Popper, who maintained the very highest research standards throughout his long and exceptionally productive career and who was known and respected for his very careful and critical approach to science, clearly felt that the unexpected discoveries to be made by interferometry will be the true hallmarks of the field.

1.3 Towards the Future

The current generation of projects may be the stepping-stones to an “Optical/IR Very Large Array.” For this to happen, significant science must be forthcoming in the near term from our present investment in the field. In this context, “significant” implies quality as well as quantity in support of pressing problems in stellar astrophysics. Imaging of relatively complex objects must be demonstrated, and this is a challenge due to the small number of collecting telescopes in current arrays. We can anticipate very little extragalactic results except for calibrations, based upon galactic objects. which extend to extragalactic realms and into cosmology. The field needs more partnerships to pool intellectual and financial resources, more involvement of theorists, and the training of more “black-belt” interferometrists.

One might look forward to great successes from present-day efforts so that by, say 2010, considerable momentum will exist towards the design and construction of an interferometer comprised of several dozen 4–6 meter aperture telescopes (each equipped with adaptive optics) distributed over kilometer-plus baselines. At that time, interferometry will truly have come of age and the words of Dan Popper will entice us to new realms of exploration and discovery.

Chapter 2

Elementary Theory of Interferometry

A.F. BODEN

IPAC, CALIFORNIA INSTITUTE OF TECHNOLOGY, AND
JET PROPULSION LABORATORY
PASADENA, CALIFORNIA

We introduce and discuss the elementary theory of astronomical interferometry. We derive the basic quantitative formalism for interferometric observables from incoherent astronomical sources with a particular emphasis upon optical interferometry. Concrete examples of the theory are given in the context of common model source morphologies.

2.1 Introduction

It is deceptively simple to describe interferometers as instruments that measure interference (or other properties associated with the interference) of an electromagnetic field. The motivation to consider interferometry of astronomical sources is fundamentally pragmatic; we are compelled to consider astronomical interferometers because interferometers provide access to high angular resolution information at a small fraction of the price of conventional single-aperture telescopes with similar angular resolution. This is not to suggest that interferometers replace more conventional astronomical instrumentation, only that they provide a cost-effective means to address certain scientific questions.

Herein we will introduce and develop the basic theory of astronomical interferometry. Starting from general properties of the electromagnetic field, we will consider the response of an idealized interferometer to idealized astronomical sources. We will further apply this theory to common idealized source morphologies. Given the context in which these lecture notes appear, we will primarily make these developments with optical interferometers in

mind; interferometers that operate over finite pass-bands in the optical (or near-optical) part of the electromagnetic spectrum. Optical astronomical interferometers have historically been used to study stars—a natural match given most stars emit a large fraction of their radiation at optical (near-optical) wavelengths.

2.2 A Simple Interferometer and a Monochromatic Source

Consider a model two-aperture interferometer as depicted in Figure 2.1. Two identical apertures A_1 and A_2 are located at three-space positions \mathbf{x}_1 and \mathbf{x}_2 respectively, and thus are separated by a displacement $\mathbf{B} \equiv \mathbf{x}_2 - \mathbf{x}_1$. \mathbf{B} is typically known as the *baseline* of the interferometer. Each aperture is pointed at a single celestial point source located at relative position \mathbf{S} from the centerline of the array pair; the pointing direction is given by the unit vector $\hat{\mathbf{s}} \equiv \mathbf{S}/|\mathbf{S}|$. Because optical photons (to an extremely good approximation) do not interact with each other, in analyzing the interferometer we can consider the harmonic decomposition of the light from the astronomical source. We therefore start by considering the source as monochromatic with wavelength λ . We'll also assume the celestial source is a sufficient distance that the phase-fronts of the incident optical radiation field are planar. At positions \mathbf{x}_1 and \mathbf{x}_2 the monochromatic optical fields from the source have a simple form as (the real part of) an exponential.*:

$$\phi_1 \sim e^{i\mathbf{k}\cdot\mathbf{x}_1} e^{-i\omega t} = e^{-ik\hat{\mathbf{s}}\cdot\mathbf{x}_1} e^{-i\omega t}$$

and

$$\begin{aligned} \phi_2 \sim e^{i\mathbf{k}\cdot\mathbf{x}_2} e^{-i\omega t} &= e^{-ik\hat{\mathbf{s}}\cdot\mathbf{x}_2} e^{-i\omega t} \\ &= e^{-ik\hat{\mathbf{s}}\cdot\mathbf{x}_1} e^{-ik\hat{\mathbf{s}}\cdot\mathbf{B}} e^{-i\omega t}. \end{aligned}$$

Without loss of generality we can absorb the common phase factor $e^{-ik\hat{\mathbf{s}}\cdot\mathbf{x}_1}$ into whatever normalization we choose for the optical fields, hence:

$$\begin{aligned} \phi_1 &\sim e^{-i\omega t}, \\ \phi_2 &\sim e^{-ik\hat{\mathbf{s}}\cdot\mathbf{B}} e^{-i\omega t}. \end{aligned} \tag{2.1}$$

Equation 2.1 merely codifies the fact that the relative phase of the radiation incident on the two apertures is a function of the geometry of the viewing situation—in particular the relative angle of the incoming phase fronts and the baseline vector \mathbf{B} .

*Herein, in so far as possible, we take our nomenclature for electromagnetic fields from Jackson (1998) In particular, a plane parallel monochromatic electromagnetic field of frequency ν propagating in free space in a direction $\hat{\mathbf{n}}$ is written as:

$$\phi \sim A e^{i(\mathbf{k}\cdot\mathbf{x} - \omega t)},$$

with

$$\begin{aligned} \omega &= 2\pi\nu = 2\pi c/\lambda, \\ k &= \omega/c = 2\pi\nu/c, \\ \mathbf{k} &= k\hat{\mathbf{n}}, \end{aligned}$$

and \mathbf{k} (k) as the wave vector (number) of the field. Consult Jackson (1998) Chapter 7 for additional details.

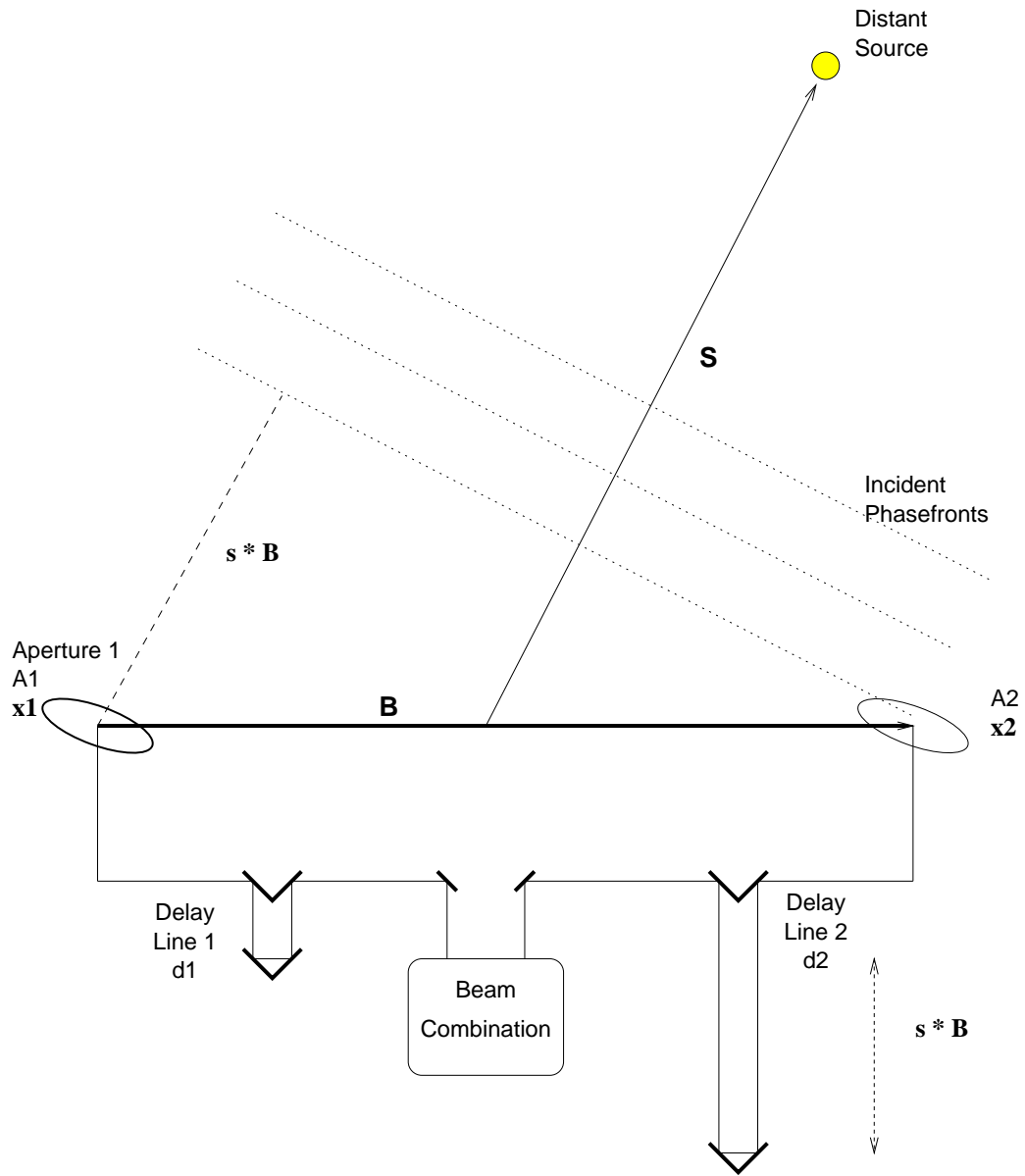


Figure 2.1: Idealized Interferometer.

As shown in Figure 2.1, we imagine that after collection the optical fields are propagated to a power-linear detector where they combined, and the resulting output is measured. Post-collection the optical fields are propagated over distinct distances d_1 and d_2 , incurring an additional relative phase. Imagining that the optical fields are directly combined, at the detector the fields have phases that are:

$$\begin{aligned}\phi_1 &\sim e^{ikd_1} e^{-i\omega t}, \\ \phi_2 &\sim e^{ikd_2} e^{-ik_0 \hat{\mathbf{s}} \cdot \mathbf{B}} e^{-i\omega t}.\end{aligned}\tag{2.2}$$

With no significant efficiency differences in the two interferometer arms, a direct[†] combination of the two optical fields results in a net field whose phase is given by:

$$\phi_{net} = \phi_1 + \phi_2 \sim e^{-i\omega t} \left(e^{ikd_1} + e^{ikd_2} e^{-ik\hat{\mathbf{s}} \cdot \mathbf{B}} \right),$$

from which the resulting time-averaged detected power is (proportional to):

$$P \propto \phi_{net}^* \phi_{net} = 2(1 + \cos k(\hat{\mathbf{s}} \cdot \mathbf{B} + d_1 - d_2)).$$

To be more concrete, let us specify the incident source flux power F in units of energy incident per unit time per unit cross-sectional area, and the collecting area of the apertures as A . Then (up to efficiency factors) the detected power is given by:

$$P = 2AF(1 + \cos k(\hat{\mathbf{s}} \cdot \mathbf{B} + d_1 - d_2))\tag{2.3}$$

$$= 2AF(1 + \cos kD).\tag{2.4}$$

In the space of relative delay $D \equiv \hat{\mathbf{s}} \cdot \mathbf{B} + d_1 - d_2$, P varies harmonically between zero and $2AF$ (the total collected power of the two apertures) with period λ ; this is plotted in Figure 2.2.

Equation 2.3 has the form of an infinite series of power oscillations or *interference fringes*, as a function of the optical delay D , or equivalently $d_1 - d_2$. Because $\hat{\mathbf{s}}$ can be interpreted as an angle on the sky with dimensions of radians, adjacent fringe crests projected on the sky are separated by an angle given by:

$$\Delta s = \frac{\lambda}{B}.\tag{2.5}$$

2.3 Polychromatic Sources and Interferometers of Finite Bandwidth

The interference fringes in Equation 2.3 were infinite; we saw interference regardless of the values of d_1 and d_2 . From a practical standpoint life is not quite this kind. In general we

[†]Direct combination in this context means combination without additional phase asymmetry between the two arms. This is an idealization which simplifies the mathematics at the expense of ignoring a relatively unimportant phase factor present in most optical interferometers which use beam splitters for beam combination.

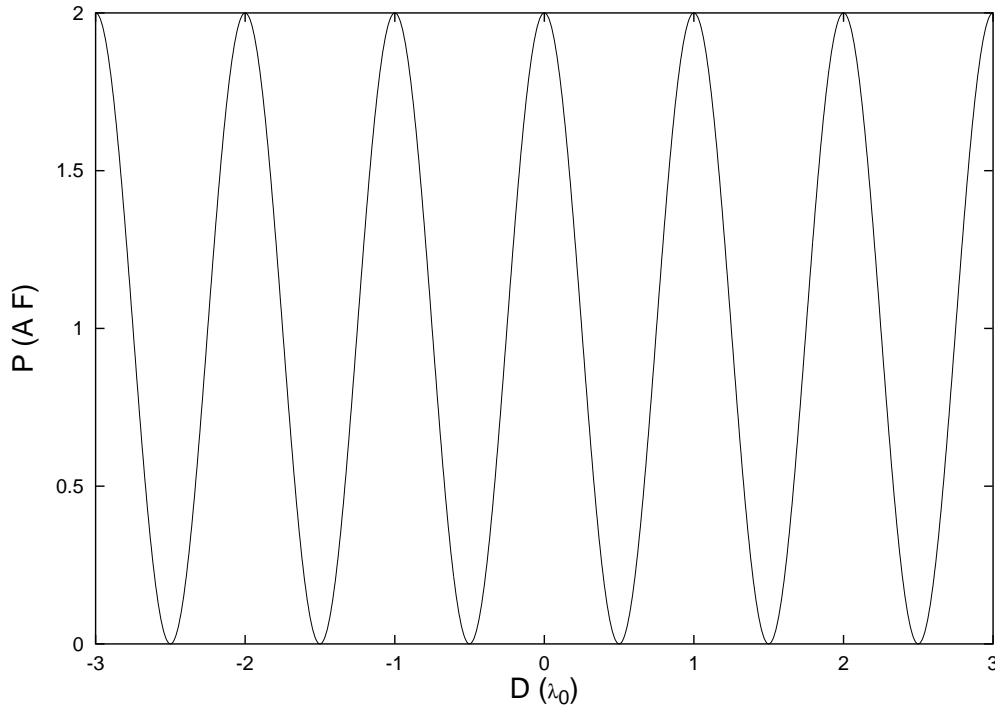


Figure 2.2: Monochromatic Power.

can only build interferometers with finite passbands, and this causes some headaches. Let's see how this goes.

Consider now a more general source with spectral intensity F_ν (dimensions of incident power per cross-sectional area per unit frequency), and an interferometer that has a finite frequency response given by $\eta(\nu)$. Because astronomical sources give us individual frequencies that are mutually incoherent, the total detected power becomes a sum of the detected power at each frequency after Equation 2.3 (writing the integration in the frequency domain):

$$P = \int d\nu 2AF_\nu \eta(\nu) [1 + \cos kD]. \quad (2.6)$$

It is illustrative to consider a specific instance. First, as a simplifying assumption we take the source spectral power to be constant, $F_{\nu-0}$, over the system bandwidth. Next, take a specific bandwidth pattern—a “top hat” pattern with constant throughput η_0 over a frequency (wavelength) band $\nu_0 \pm \Delta\nu/2$ ($\lambda_0 \pm \Delta\lambda/2$). Then Equation 2.6 becomes:

$$\begin{aligned} P &= 2AF_{\nu-0}\eta_0 \int_{\nu_0-\Delta\nu/2}^{\nu_0+\Delta\nu/2} d\nu (1 + \cos 2\pi\nu\tau) \\ &= 2AF_{\nu-0}\eta_0 \left[\nu + \frac{\sin 2\pi\nu\tau}{2\pi\tau} \right]_{\nu_0-\Delta\nu/2}^{\nu_0+\Delta\nu/2} \\ &= 2AF_{\nu-0}\eta_0\Delta\nu \left[1 + \frac{\sin \pi\Delta\nu\tau}{\pi\Delta\nu\tau} \cos 2\pi\nu_0\tau \right] \end{aligned}$$

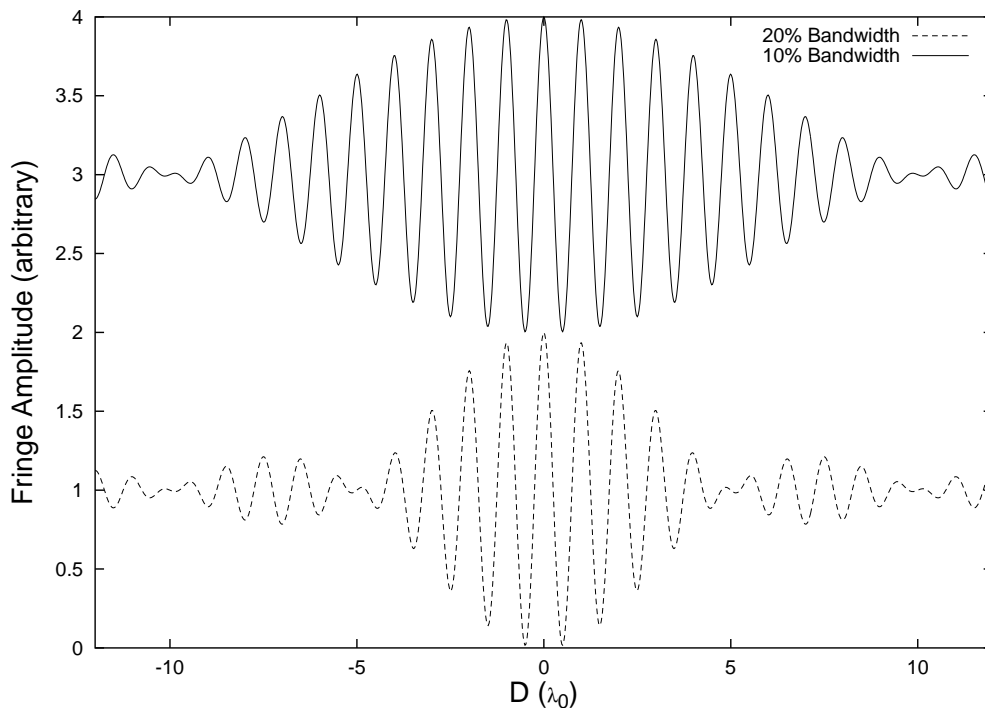


Figure 2.3: Polychromatic Fringe Coherence.

$$\begin{aligned}
 &= 2AF_{\lambda-0}\eta_0\Delta\lambda \left[1 + \frac{\sin \pi\Delta\lambda/\lambda_0^2 D}{\pi\Delta\lambda/\lambda_0^2 D} \cos k_0 D \right] \\
 &= 2AF_{\lambda-0}\eta_0\Delta\lambda \left[1 + \frac{\sin \pi D/\Lambda_{coh}}{\pi D/\Lambda_{coh}} \cos k_0 D \right] \quad (2.7)
 \end{aligned}$$

(with $\tau \equiv D/c$ —dimensions of time). This result is qualitatively similar to Equation 2.3. First it is noteworthy that the leading coefficient of Equation 2.7 is the total collected power by both apertures in a bandwidth $\Delta\nu$ (with efficiency η_0). Further, as in Equation 2.3 the term in brackets has a positive-definite oscillatory behavior in D at a frequency ν_0 /wavelength λ_0 —the center-band frequency. But rather than the fringes being observed at all D as suggested by Equation 2.3, we find the fringes modulated by a sinc function symmetrically centered at $D = 0$, and becoming small as $|\pi\Delta\lambda/\lambda_0^2 D| > 1$. The sinc-modulation of the interference fringes has a characteristic scale or *coherence length* of:

$$\Lambda_{coh} \equiv \frac{\lambda_0^2}{\Delta\lambda}. \quad (2.8)$$

It is noteworthy that the sinc function is the Fourier transform of the top-hat function we took for the system bandpass.

In Figure 2.3 we give two illustrative examples of the oscillatory argument of Equation 2.7, showing fringe patterns at 20% (red— $\Lambda_{coh} = 5\lambda_0$) and 10% (blue— $\Lambda_{coh} = 10\lambda_0$) fractional bandwidths.

Equation 2.7 and Figure 2.3 are typical of the types of fringe envelopes that one can expect from stellar interferometers; it is usually a reasonable first approximation to assume both the source spectral flux and the system throughput are quasi-constant over a finite frequency (wavelength) interval.

The fringe envelopes from interferometers can typically be written as:

$$1 + M(\Lambda_{coh}, D) \cos k_0 D, \quad (2.9)$$

where $M(\Lambda_{coh})$ is the fringe envelope modulation function, typically given by the Fourier transform (modulus) of the system bandpass, and k_0 is the (possibly weighted) center-band wave number. In this context Λ_{coh} sets the physical scale for the precision with which the delays must be matched in the interferometer. Conversely, if it can be measured the relative delay $d_1 - d_2$ becomes a proxy for the source astrometry (Shao *et al.* 1990).

2.4 Phase Reference of the Interferometer; Off-Axis and Extended Sources

In general the response of the interferometer to a point-source at location $\hat{\mathbf{s}}_0$ in the sky is given by something like Equation 2.7; fringes with frequency ω_0 modulated by a fringe envelope that is a function of the system bandwidth (in delay space). In particular, we see the fringe envelope position is given by the product $k_0 D = k_0(\hat{\mathbf{s}}_0 \cdot \mathbf{B} + d_1 - d_2)$, and we are motivated to minimize this product. It is conventional to *define* (or control) the relative delay $d_2 - d_1$ to be equal to (a model of) $\hat{\mathbf{s}}_0 \cdot \mathbf{B}$, then we are guaranteed we are at maximum of the fringe envelope function for a source at $\hat{\mathbf{s}}_0$. In this context $\hat{\mathbf{s}}_0$ becomes our *phase reference* or *phase tracking center*.

Now we can ask what is the response from a point source at $\hat{\mathbf{s}}$ offset slightly from the reference position $\hat{\mathbf{s}}_0$:

$$\hat{\mathbf{s}} = \hat{\mathbf{s}}_0 + \Delta \mathbf{s}.$$

If we write the fringe envelope function as $M(\Lambda_{coh}, \Delta D)$ (which goes to unity in the monochromatic limit), the output power from the interferometer is (after Equation 2.3):

$$\begin{aligned} P &= 2AF (1 + M(\Lambda_{coh}, \Delta D) \cos k_0(\hat{\mathbf{s}} \cdot \mathbf{B} - \hat{\mathbf{s}}_0 \cdot \mathbf{B})) \\ &= 2AF (1 + M(\Lambda_{coh}, \Delta D) \cos k_0(\Delta \mathbf{s} \cdot \mathbf{B})) \\ &= 2AF (1 + M(\Lambda_{coh}, \Delta D) \cos k_0(\Delta D)), \end{aligned} \quad (2.10)$$

with $\Delta D \equiv \Delta \mathbf{s} \cdot \mathbf{B}$. In this construction the sky position $\hat{\mathbf{s}}_0$ as defined by the relative delay $d_2 - d_1$ *defines* the phase reference of the interference fringes on the sky[‡].

[‡]In fact, the relative delay $d_2 - d_1$ defines a *circle* on the celestial sphere around the baseline vector \mathbf{B} . The peak of the optical aperture reception pattern $A(\hat{\mathbf{s}})$ breaks the circular symmetry of the dot product and defines the phase reference $\hat{\mathbf{s}}_0$.

Extended Sources

Any source with finite surface temperature has the potential for being resolved, so we must consider the possibility of resolved sources. Let's describe the source intensity as a function of position $\hat{\mathbf{s}}$ in the sky as $F(\hat{\mathbf{s}})$. Typically F has units of power incident per unit area per solid angle on the sky, and for the moment let's take this with respect to one particular wavelength λ . It is also necessary to characterize the throughput or collection efficiency of the interferometer telescopes as a function of sky position. In terms of what we've had before we'll write this as $A(\hat{\mathbf{s}}, \hat{\mathbf{s}}_0)$, assuming that the telescopes are boresighted on the phase tracking center $\hat{\mathbf{s}}_0$. It is convenient to take the units of A to be effective cross-sectional area, such that a product of $A(\hat{\mathbf{s}}, \hat{\mathbf{s}}_0)F(\hat{\mathbf{s}}) d\Omega$ forms a received power differential.

In the assumption that the radiation from different locations on the source is incoherent, the detected power from an extended source can be computed as an incoherent sum of power from the source decomposed into infinitesimal point sources. Such a model can be written a straightforward extension of the point source model from Equation 2.10:

$$\begin{aligned} P(\hat{\mathbf{s}}_0, \mathbf{B}) &= \int d\Omega A(\hat{\mathbf{s}}, \hat{\mathbf{s}}_0)F(\hat{\mathbf{s}}, \hat{\mathbf{s}}_0) (1 + M(\Lambda_{coh}, \Delta D) \cos k(\Delta\mathbf{s} \cdot \mathbf{B})) \\ &\rightarrow \int d\Omega A(\Delta\mathbf{s})F(\Delta\mathbf{s}) (1 + \cos k(\Delta\mathbf{s} \cdot \mathbf{B})), \end{aligned} \quad (2.11)$$

where I have suppressed the factor of 2 into the magnitude of A , and dropped the envelope function as a notational convenience, regressing to a monochromatic source.

It is interesting, and in fact evocative of how optical interferometers measure fringes in practice, to consider the detected power when a small additional phase is added to one of the delay line arms. To be definite, let's call the delay offset δ with dimensions of length like D , and define it to be positive when a positive delay is added to delay line 1. In this case the detected power becomes:

$$\begin{aligned} P(\hat{\mathbf{s}}_0, \mathbf{B}, \delta) &= \int d\Omega A(\Delta\mathbf{s})F(\Delta\mathbf{s}) (1 + \cos k(\Delta\mathbf{s} \cdot \mathbf{B} + \delta)) \\ &= \int d\Omega A(\Delta\mathbf{s})F(\Delta\mathbf{s}) \\ &\quad + \cos k\delta \int d\Omega A(\Delta\mathbf{s})F(\Delta\mathbf{s}) \cos k(\Delta\mathbf{s} \cdot \mathbf{B}) \\ &\quad - \sin k\delta \int d\Omega A(\Delta\mathbf{s})F(\Delta\mathbf{s}) \sin k(\Delta\mathbf{s} \cdot \mathbf{B}). \end{aligned} \quad (2.12)$$

It is conventional to introduce the *complex visibility* V of the brightness distribution B with respect to the phase reference $\hat{\mathbf{s}}_0$ and aperture function A as:

$$V(k, \mathbf{B}) \equiv \int d\Omega A(\Delta\mathbf{s})F(\Delta\mathbf{s})e^{-ik\Delta\mathbf{s} \cdot \mathbf{B}}. \quad (2.13)$$

Using V we can write the detected power concisely as:

$$\begin{aligned} P(\hat{\mathbf{s}}_0, \mathbf{B}, \delta) &= \int d\Omega A(\Delta\mathbf{s})F(\Delta\mathbf{s}) + Re\{V\} \cos k\delta + Im\{V\} \sin k\delta \\ &= P_0 + Re\{Ve^{ik\delta}\}, \end{aligned} \quad (2.14)$$

where I have written the (two) aperture-integrated power as a constant P_0 :

$$P_0 \equiv \int d\Omega A(\Delta\mathbf{s})F(\Delta\mathbf{s}).$$

To see why Equation 2.14 is considered progress, let's look a little closer at V . To make things definite, let's take a coordinate system where $\hat{\mathbf{s}}_0 = (0, 0, 1)$. So long as either the field of view of the interferometer telescopes is small or the the source brightness is of limited angular extent, $\Delta\mathbf{s}$ is approximately perpendicular to $\hat{\mathbf{s}}_0$ and can be written in terms of angles α and β (units of radians):

$$\Delta\mathbf{s} \approx (\alpha, \beta, 0),$$

and the visibility becomes:

$$V(k, \mathbf{B}) = \int d\alpha d\beta A(\alpha, \beta) F(\alpha, \beta) e^{-ik(\alpha B_x + \beta B_y)}.$$

It is further conventional to define *spatial frequencies* u and v [§]:

$$\begin{aligned} u &\equiv \frac{B_x}{\lambda} = \frac{kB_x}{2\pi}, \\ v &\equiv \frac{B_y}{\lambda} = \frac{kB_y}{2\pi}, \end{aligned} \tag{2.15}$$

for which V becomes:

$$V(u, v) = \int d\alpha d\beta A(\alpha, \beta) F(\alpha, \beta) e^{-2\pi i(\alpha u + \beta v)}. \tag{2.16}$$

As written, $V(u, v)$ is a complex quantity with dimensions of power (as given by the product of A and F).

2.5 Image Synthesis by Discrete Visibility Measurements

The form of Equation 2.16 is clearly that of a two-dimensional Fourier transform of the (aperture efficiency modulated) brightness distribution with u and v assuming roles of spatial frequencies (units of fringe cycles per radian on the sky). That the interferometer response is related to the Fourier transform of the brightness distribution under certain assumptions (source incoherence, small-field approximation) is typically known as the van Cittert–Zernike theorem; the interested reader can find more thorough discussions of the van Cittert–Zernike theorem in Born and Wolf (1999) and Thompson, Moran, and Swenson (1986).

[§]It is further conventional to orient coordinates so u and v represent spatial frequencies in convenient astronomical coordinates like right ascension and declination, but for the present purpose our choice of coordinate rotation is arbitrary

Since Fourier transforms are straightforwardly invertible, the visibility (provided we can measure it) can be used to compute the source brightness distribution:

$$F(\alpha, \beta) = \left(\int du dv V(u, v) e^{2\pi i(\alpha u + \beta v)} \right) / A(\alpha, \beta). \quad (2.17)$$

Equation 2.17 suggests the canonical synthesis imaging program: collect a set of visibility measurements that in some sense approximate the visibility surface over the (u, v) coordinate plane. In practice a set of discrete interferometer baselines \mathbf{B}_i targeted on a common phase-tracking center $\hat{\mathbf{s}}_0$ yields a set of discrete visibility measurements $V_i(u_i, v_i)$. This discrete visibility field can then be inverted by means of a discrete Fourier transform operation to obtain a bandwidth-limited estimate of the parent brightness distribution. The accuracy of the synthesized image is naturally a function of the coverage of the (u, v) plane.

To be concrete, we can describe a sampling function $S(u, v)$ that has the form of a sum of delta functions at the sampled locations (u_i, v_i) :

$$S(u, v) \equiv \sum_i \delta(u - u_i) \delta(v - v_i). \quad (2.18)$$

Utilizing this sampling function Equation 2.17 can be written:

$$F_d(\alpha, \beta) = \left(\int du dv V(u, v) S(u, v) e^{2\pi i(\alpha u + \beta v)} \right) / A(\alpha, \beta). \quad (2.19)$$

Radio Astronomers typically refer to F_d as the *dirty* brightness distribution or image, in that it is apparently related to the true brightness distribution F by the convolution of an effective point-spread function (PSF) or synthesized beam*:

$$F_d(\alpha, \beta) = F(\alpha, \beta) * p(\alpha, \beta),$$

with

$$p(\alpha, \beta) = \int du dv S(u, v) e^{2\pi i(u\alpha + v\beta)}.$$

For our discussion suffice it to say that there are deconvolutional methods to estimate $F(\alpha, \beta)$ from $F_d(\alpha, \beta)$ and $p(\alpha, \beta)$ in the presence of noise; the interested reader is referred to the NRAO Summer School Proceedings (Perley *et al.*, 1989).

2.6 Visibilities of Various Flavors and Their Physical Interpretations

The development of Equation 2.13 might leave the reader with an impression that fringe visibility is a mathematical artifice useful only for image inversion. This is incorrect, and it is instructive to consider the properties of the visibility in a physical context as well as a mathematical one.

*Convolution in the spatial domain is multiplication in the spatial frequency domain

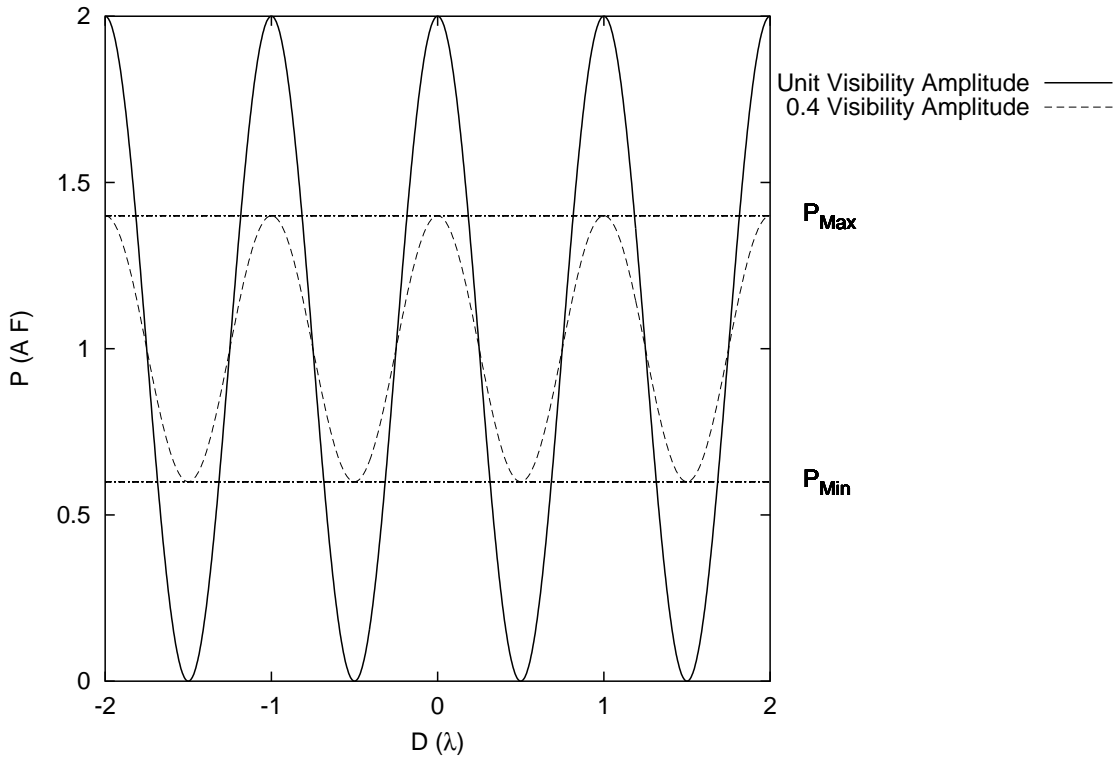


Figure 2.4: Normalized Visibility Amplitude (Michelson Visibility).

First, we remind the reader that as defined to this point the visibility is *dimensional*—it has dimensions of power (Equations 2.13 and 2.16). In fact, the form of Equation 2.14 makes it clear that the modulus or *amplitude* of the complex visibility describes the amount of power the interferometer measures in delay-space fringes. In the sense we used the word in the introduction, the visibility quantitatively captures the coherent response of the interferometer to the astronomical source. In the sense of language used in the development of the van Cittert–Zernike theorem, the visibility captures (one component of) the spatial coherence function of the astronomical source.

Optical interferometers typically measure the normalized fringe power, the fringe power *relative* to the total power collected from the source. For instance, in his classical studies on stellar diameters at Mt. Wilson, Michelson (Michelson, 1920; Michelson and Pease, 1921) defined the visibility of his fringes as the apparent contrast between light and dark areas (power P_{Max} and P_{Min} respectively) of fringes visible in his telescope eyepiece. This is quantified as the Michelson fringe visibility

$$\mathcal{V}_M \equiv \frac{P_{\text{Max}} - P_{\text{Min}}}{P_{\text{Max}} + P_{\text{Min}}},$$

which, of course, is dimensionless and contained in the interval $[0,1]$. Michelson’s construction is depicted in Figure 2.4. As we will demonstrate below, for sources that are unresolved to the interferometer the fringes oscillate with a peak-to-peak amplitude of the full received power ($2AF$). As the source increases in apparent size they become resolved by the in-

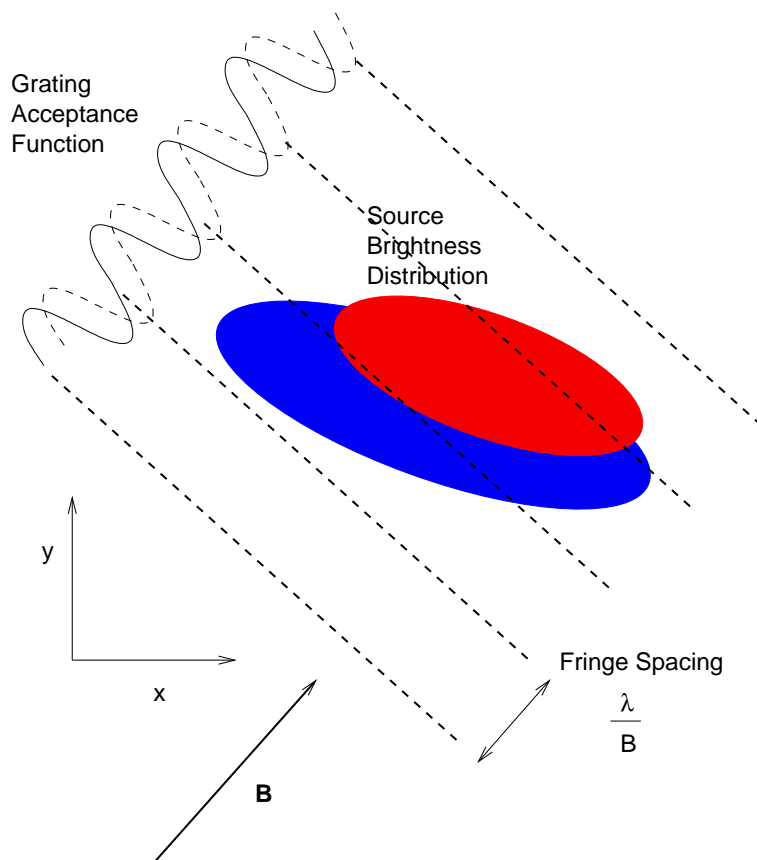


Figure 2.5: Interferometer Response to Extended Source.

terferometer and the fringes decrease in amplitude. We shall make these statements more quantitative in Section 2.7.

Following Michelson's example, we commonly work in a normalized, dimensionless visibility, given as an extension of Equation 2.13:

$$\mathcal{V}(k, \mathbf{B}) \equiv \frac{\int d\Omega A(\Delta\mathbf{s})F(\Delta\mathbf{s})e^{-ik\Delta\mathbf{s}\cdot\mathbf{B}}}{\int d\Omega A(\Delta\mathbf{s})F(\Delta\mathbf{s})} = \frac{V(k, \mathbf{B})}{P_0}, \quad (2.20)$$

in which case the detected power given by Equation 2.14 takes the form.

$$P = P_0 \left(1 + \text{Re}\{\mathcal{V}e^{ik\delta}\} \right). \quad (2.21)$$

Comparison of the Michelson visibility and Equation 2.21 makes it clear that $\mathcal{V}_M = |\mathcal{V}|$; the modulus of \mathcal{V} is similarly contained in the interval $[0,1]$.[†]

Figure 2.5 gives a depiction of how I think of the interferometric visibility. Given some arbitrary source intensity distribution on the sky, the instantaneous interferometer response/visibility is given by a sum of the received power from the source multiplied by

[†]This had to be true—the modulus of the exponential kernel in Equation 2.20 is contained in the interval $[0,1]$, and we normalize by the received power from the source.

a cosine grating acceptance function referenced to the instantaneous phase center. This grating function oscillates along the (projected) baseline direction with angular frequency λ/B , and is constant in the direction normal to the baseline (up to the angular extent defined by the collecting aperture acceptance function A). The grating function is further multiplied by a fringe coherence envelope along the baseline direction in the polychromatic case; this is not shown in the figure. A small change in the path difference between the two arms of the interferometer translates the phase tracking center and shifts the reference point of the grating acceptance function, with corresponding changes in the received fringe power. Both the baseline direction and angular frequency of the fringes in the grating acceptance function are conveniently captured in the spatial frequencies u and v .

In terms of predicting the response of the interferometer, rather than evaluating this grating-modulated source distribution over some continuum of phase centers, we find it quantitatively convenient to describe the morphology of the source in terms of a complex visibility that simultaneously captures both the even (cosine) and odd (sine) components of the source morphology relative to a fixed phase center. This is given not by the real, cosine grating function, but by a complex exponential grating function containing both even and odd components. When the interferometer is phased at the reference center it responds to the even (cosine) component, and when it is phased $\pm\pi/2$ radians away from the reference center it responds to the odd (sine) component. Between these two situations the interferometer sees an admixture of the even and odd components.

As a final remark for readers familiar with the mathematics of quantum mechanics, I have often found it constructive to think of the interferometer grating acceptance function as a particular basis vector in an Hilbert space, with the interferometer response in any given configuration given by a projection of the source brightness distribution onto the particular Hilbert basis vector. Like quantum mechanics, a full description of a general source morphology requires both even and odd components in the space. In this analogy the act of image synthesis reduces to estimating the properties of the source morphology having measured some (finite) set of these Hilbert components, and employing some *a priori* knowledge of the source morphology (e.g. positivity, bandwidth limitations, etc.). Perhaps someday I'll develop this analogy with quantum mechanics further in the context of a monograph.

2.7 Visibility of Common Source Morphologies

To close our discussion it is interesting and constructive to consider the visibilities of some of the more common source morphologies. It serves to codify application of the visibility formalism developed above, and we can discuss some of the general properties of interferometric visibility in the context of applications. Further, for optical interferometry these developments are instructive and necessary to interpret observations. We will, characteristically, be dealing with some idealized examples amenable to analytical treatment (cf.

Michelson 1890). However, these offer significant insight into the strengths and weaknesses of the interferometer as an imaging instrument.

2.7.1 Point Source

Many sources are sufficiently distant and isolated that they may be considered point-like, or at least approximately so. To close the loop on our original calculations as well as providing a point of departure for multiple sources systems it is interesting to treat the point source within the visibility framework.

The brightness distribution of a point source at source coordinates (α_0, β_0) relative to the phase reference is simple to write down in terms of Dirac delta functions:

$$F_0 \delta(\alpha - \alpha_0) \delta(\beta - \beta_0).$$

The total collected power from such a source is:

$$P_0 = \int d\alpha d\beta A(\alpha, \beta) F_0 \delta(\alpha - \alpha_0) \delta(\beta - \beta_0) = A(\alpha_0, \beta_0) F_0.$$

The complex visibility of such a point source is computed after Equation 2.16 as:

$$\begin{aligned} V(u, v) &= \int d\alpha d\beta A(\alpha, \beta) F_0 \delta(\alpha - \alpha_0) \delta(\beta - \beta_0) e^{-2\pi i(\alpha u + \beta v)} \\ &= A(\alpha_0, \beta_0) F_0 e^{-2\pi i(\alpha_0 u + \beta_0 v)} = P_0 e^{-2\pi i(\alpha_0 u + \beta_0 v)} \end{aligned} \quad (2.22)$$

the total received power times a phase. Of course, the normalized visibility for the point source is trivially:

$$\mathcal{V} = e^{-2\pi i(\alpha_0 u + \beta_0 v)}, \quad (2.23)$$

a pure phase—of course. Note that for the on-axis (on-reference) source α_0 and β_0 are zero, and the normalized visibility is unity. Of course, the normalized visibility amplitude (modulus) of the point source is always unity.

To compute the interferometer detected power for this source we can insert the complex visibility, Equation 2.22 (normalized visibility, Equation 2.23) into the detected power equation, Equation 2.14 (Equation 2.21), yielding:

$$\begin{aligned} P &= P_0 \left(1 + \text{Re}\{e^{-2\pi i(\alpha_0 u + \beta_0 v)} e^{ik\delta}\} \right) \\ &= P_0 \left(1 + \text{Re}\{e^{-ik\mathbf{\Delta s} \cdot \mathbf{B}} e^{ik\delta}\} \right) \\ &= P_0 (1 + \cos k(\mathbf{\Delta s} \cdot \mathbf{B})), \end{aligned} \quad (2.24)$$

where we have identified (α_0, β_0) with $\mathbf{\Delta s}$, and set $\delta = 0$ in the last equality to demonstrate consistency with Equation 2.10.

2.7.2 Uniform Disk

Longer interferometric baselines offer unprecedented angular resolution—so much resolution in fact that sources conventionally taken as point sources become resolved. One important class of such objects is nearby stars; resolving and measuring the angular diameters of stars is one of the bread-and-butter science topics for optical interferometers (Michelson and Pease, 1921; Hanbury Brown *et al.*, 1974; Mozurkewich *et al.*, 1991; van Belle *et al.*, 1999).

A reasonable approximation to the brightness distribution of a resolved star is the model of a uniform disk. (Interesting physics arises from considering deviations from the uniform disk model; Quirrenbach *et al.* (1996); Hajian *et al.* (1998) discuss stellar limb darkening as measured by optical interferometers.) We can write the model for an axisymmetric disk in terms of polar coordinates as:

$$F(\rho) = F_0(\rho < \theta/2),$$

ρ being an angular offset on the celestial sphere away from the nominal center of the source, and θ being the diameter of the source. In such a model the total power collected from the source is trivially $P_0 = A_0 F_0 \pi \theta^2 / 4$ —this in fact defines the value of the surface brightness F_0 (dimensions of incident power per square angle on the sky per collecting area). After Equation 2.16 (and assuming the angular extent of the disk is much smaller than the angular size of the aperture response function), the complex visibility of the disk at source position (α_0, β_0) is:

$$V(u, v) = e^{-2\pi i(\alpha_0 u + \beta_0 v)} \int d\alpha d\beta A_0 F e^{-2\pi i(u\alpha + v\beta)},$$

where we have taken advantage of the phase property of the Fourier transform under coordinate translations to arrange convenient integration variables; we saw an example of this phase property for the point source in Equation 2.22.

Fourier Transform of the Axisymmetric Function

To compute the visibility for the disk we need to consider the two-dimensional Fourier transform of an axisymmetric function. Taking $f = f(\rho)$, we wish to evaluate

$$F(u, v) = \int d\alpha d\beta f(\rho) e^{-2\pi i(u\alpha + v\beta)} = \int d\rho d\theta \rho f(\rho) e^{-2\pi i\rho(u \cos \theta + v \sin \theta)},$$

with $\alpha = \rho \cos \theta$ and $\beta = \rho \sin \theta$. It is convenient to drop u and v in favor of some angular spatial frequency variables:

$$u \equiv v_r \cos \phi, \quad v \equiv v_r \sin \phi,$$

v_r is a radial spatial frequency; like u and v it has dimensions of fringe cycles per radian on the sky. In this transformation F becomes:

$$F(v_r, \phi) = \int d\rho d\theta \rho f(\rho) e^{-2\pi i\rho v_r (\cos \theta \cos \phi + \sin \theta \sin \phi)} = \int d\rho d\theta \rho f(\rho) e^{-2\pi i\rho v_r \cos(\theta - \phi)}.$$

F is by construction axially symmetric, so we are free to take $\phi = 0$ without loss of generality. The θ -integral can now be performed, as:

$$\int_0^{2\pi} d\theta e^{ix\cos\theta} = 2\pi J_0(x),$$

J_0 being the zeroth-order Bessel function of the first kind. This allows us to finally write:

$$F(v_r) = 2\pi \int_0^\infty d\rho \rho f(\rho) J_0(-2\pi\rho v_r) = 2\pi \int_0^\infty d\rho \rho f(\rho) J_0(2\pi\rho v_r) \quad (2.25)$$

as even-ordered Bessel functions are even functions and odd-ordered Bessel functions are odd functions. Equation 2.25 is the general form of a two-dimensional Fourier transform of an axially symmetric function; we have used the axial symmetry to trade the two-dimensional transform for a one-dimensional transform with a different (slightly more complicated) transform kernel. This transform is commonly known as a Hankel (or Fourier-Bessel) transform.

Back to the uniform disk, after Equation 2.25 the visibility of the disk is evidently:

$$\begin{aligned} V(v_r) &= e^{-2\pi i(\alpha_0 u + \beta_0 v)} 2\pi \int_0^{\theta/2} d\rho \rho F_0 J_0(2\pi\rho v_r) \\ &= e^{-2\pi i(\alpha_0 u + \beta_0 v)} \frac{8P_0}{\theta^2} \int_0^{\theta/2} d\rho \rho J_0(2\pi\rho v_r). \end{aligned}$$

This is straightforwardly evaluated from:

$$\int_0^x dx' x' J_0(x') = x J_1(x).$$

Then:

$$\begin{aligned} V(v_r) &= e^{-2\pi i(\alpha_0 u + \beta_0 v)} \frac{8P_0}{\theta^2} \int_0^{x=2\pi v_r \theta/2} \frac{dx x}{(2\pi v_r)^2} J_0(x) \\ &= e^{-2\pi i(\alpha_0 u + \beta_0 v)} 2P_0 \frac{J_1(\pi v_r \theta)}{\pi v_r \theta}. \end{aligned} \quad (2.26)$$

Recall v_r is a radial spatial frequency ($v_r^2 = u^2 + v^2 = B_\perp^2/\lambda^2$), making the visibility:

$$V(B_\perp, \lambda, \theta) = e^{-2\pi i(\alpha_0 u + \beta_0 v)} 2P_0 \frac{J_1(\pi\theta B_\perp/\lambda)}{\pi\theta B_\perp/\lambda}. \quad (2.27)$$

Trivially the normalized visibility is given by:

$$\mathcal{V}(B_\perp, \lambda, \theta) = e^{-2\pi i(\alpha_0 u + \beta_0 v)} \frac{2J_1(\pi\theta B_\perp/\lambda)}{\pi\theta B_\perp/\lambda}. \quad (2.28)$$

Because of noise properties, optical interferometers typically measure squared normalized visibility. Trivially the squared normalized visibility amplitude (modulus) for the uniform disk is:

$$\mathcal{V}^2(B_\perp, \lambda, \theta) = \left(\frac{2J_1(\pi\theta B_\perp/\lambda)}{\pi\theta B_\perp/\lambda} \right)^2. \quad (2.29)$$

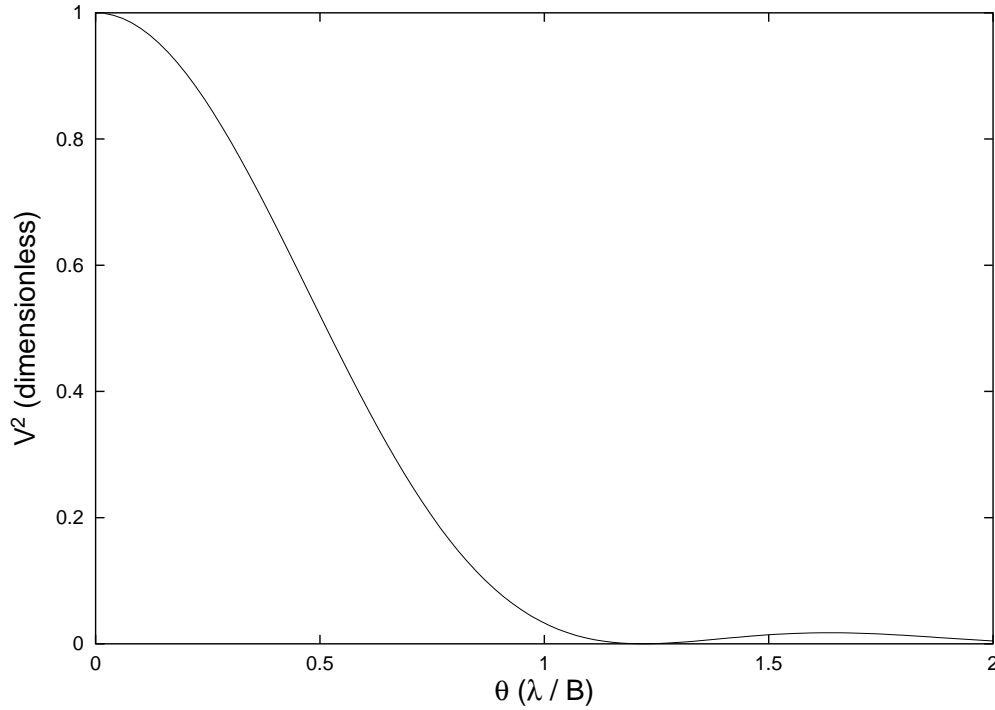


Figure 2.6: Squared Normalized Visibility Amplitude for the Uniform Disk. The disk diameter θ is plotted in units of the interferometer fringe spacing λ / B_{\perp} .

Figure 2.6 gives a plot of \mathcal{V}^2 as a function of disk diameter θ (in units of the fringe spacing λ / B_{\perp}). In the limit that the disk is much smaller than the fringe spacing $\mathcal{V}^2 \approx 1$, the disk is unresolved by the interferometer, and the visibility reduces to the results for the unresolved point source developed above. As the disk becomes an appreciable fraction of the fringe spacing the visibility \mathcal{V} becomes less than 1; in general terms we speak of a source being *resolved* by the interferometer when the normalized visibility amplitude (or \mathcal{V}^2) is measurably less than 1. The visibility actually goes to zero—fringes disappear—for the disk at a diameter of $\theta \approx 1.22 \lambda / B_{\perp}$. After this first null the fringes reappear, but at very low amplitude.

2.7.3 Multiple Stellar Systems

Nature often forms stars in multiple systems, and we are therefore motivated to consider multiple stellar systems.

We can consider the interferometer response to a multiple system as a collection of quasi-uniform stellar disks that lie in the aperture acceptance pattern. Labeling the parameters of the j th source with a subscript, up to aperture efficiency factors, the total received power from the system is simply the sum of the powers from the visible sources:

$$P_0 = \sum_j P_j.$$

Because of the linear properties of the Fourier transform (physically, because the light from the individual sources is incoherent), we can compose the system's complex visibility as the sum of the complex visibilities of the constituent disks at source positions (α_j, β_j) (Equation 2.27):

$$V = \sum_j V_j = \sum_j P_j \frac{2J_1(\pi\theta_j B_\perp/\lambda)}{\pi\theta_0 B_\perp/\lambda} e^{-2\pi i(u\alpha_j + v\beta_j)},$$

straightforwardly making the normalized visibility:

$$\mathcal{V} = \frac{\sum_j P_j \frac{2J_1(\pi\theta_j B_\perp/\lambda)}{\pi\theta_0 B_\perp/\lambda} e^{-2\pi i(u\alpha_j + v\beta_j)}}{\sum_j P_j} = \frac{\sum_j P_j \mathcal{V}_j}{\sum_j P_j}, \quad (2.30)$$

with \mathcal{V}_j given by Equation 2.28 in a uniform disk model.

Equation 2.30 doesn't offer much physical insight, therefore a concrete example is in order. Binary stars are a traditional and important target of optical interferometers (Michelson, 1920; Herbison-Evans *et al.*, 1971; Hummel *et al.*, 1995; Hummel *et al.*, 1998; Boden *et al.*, 1999), with the visibility acting as a proxy for the relative astrometry between the two components. Straightforward application of Equation 2.30 to a two component binary system yields:

$$\begin{aligned} \mathcal{V}_{\text{binary}} &= \frac{P_1 \mathcal{V}_1 + P_2 \mathcal{V}_2}{P_1 + P_2} \\ &= e^{-2\pi i(u\alpha_1 + v\beta_1)} \frac{|\mathcal{V}_1| + r |\mathcal{V}_2| e^{-2\pi i(u\Delta\alpha + v\Delta\beta)}}{1 + r}, \end{aligned} \quad (2.31)$$

having defined $r \equiv P_2/P_1$, and relative source coordinates $\Delta\alpha \equiv \alpha_2 - \alpha_1$ and $\Delta\beta \equiv \beta_2 - \beta_1$. When the observable is $\mathcal{V}_{\text{binary}}^2$, this is given straightforwardly by the squared modulus of Equation 2.31:

$$\begin{aligned} \mathcal{V}_{\text{binary}}^2 &= \mathcal{V}_{\text{binary}}^* \mathcal{V}_{\text{binary}} \\ &= \frac{\mathcal{V}_1^2 + r^2 \mathcal{V}_2^2 + 2r |\mathcal{V}_1| |\mathcal{V}_2| \cos(2\pi(u\Delta\alpha + v\Delta\beta))}{(1 + r)^2} \\ &= \frac{\mathcal{V}_1^2 + r^2 \mathcal{V}_2^2 + 2r |\mathcal{V}_1| |\mathcal{V}_2| \cos(2\pi \mathbf{B} \cdot \mathbf{s}_{\text{binary}}/\lambda)}{(1 + r)^2}, \end{aligned} \quad (2.32)$$

with $\mathbf{s}_{\text{binary}} \equiv (\Delta\alpha, \Delta\beta)$. Note that there are corrections due to finite bandwidth effects when $\mathbf{B} \cdot \mathbf{s}_{\text{binary}}$ is more than a few fringe spacings; the exact form of these corrections can depend on details of the fringe measurement process.

In the limit of point-like, equal-amplitude components $\mathcal{V}_{\text{binary}}^2$ reduces to:

$$\mathcal{V}_{\text{binary}}^2 \rightarrow \frac{1 + \cos(2\pi \mathbf{B} \cdot \mathbf{s}_{\text{binary}}/\lambda)}{2}.$$

Clearly as $\mathbf{s}_{\text{binary}} \rightarrow 0$ the two components of the binary system are unresolved by the interferometer. With increasing $\mathbf{s}_{\text{binary}}$, as $\mathbf{B} \cdot \mathbf{s}_{\text{binary}} \rightarrow \lambda/4$, $\mathcal{V}_{\text{binary}}^2 \rightarrow 1/2$, and the binary

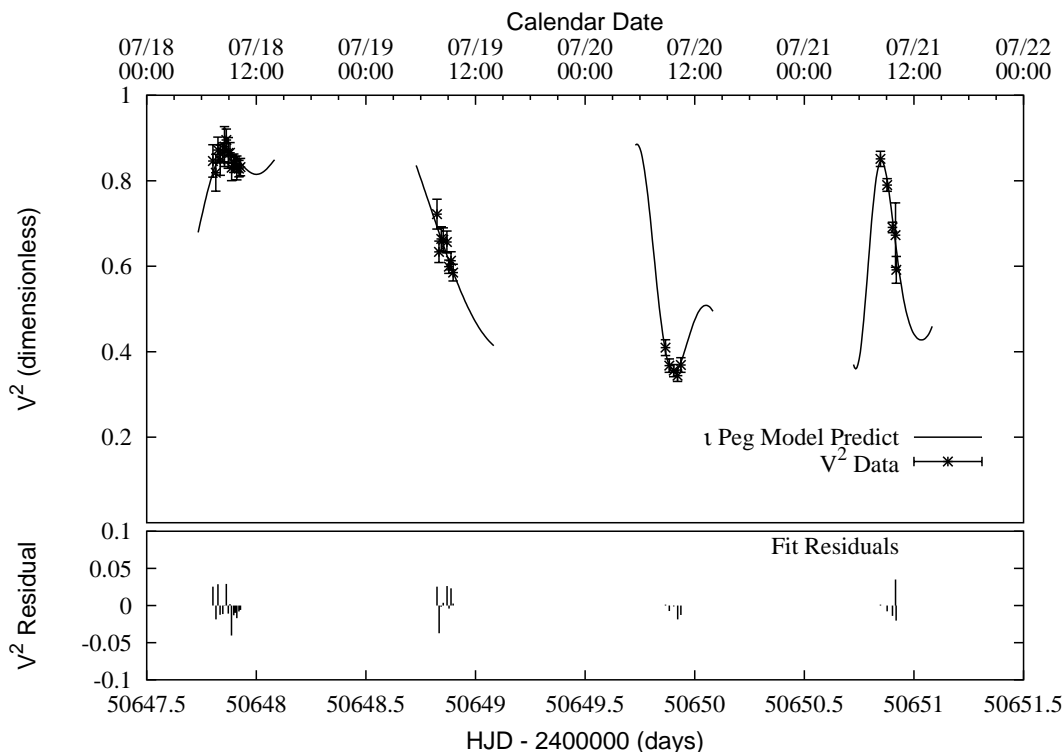


Figure 2.7: Squared Normalized Visibility Amplitude on the binary star ι Pegasi (HD 210027). Palomar Testbed Interferometer near-infrared \mathcal{V}^2 measurements of ι Peg are shown from four consecutive nights in July 1997. A model based on Equation 2.32 (and incorporating finite bandwidth effects) is fit to the \mathcal{V}^2 measurements to derive an orbit model for ι Peg (from Boden *et al.* 1999).

system becomes “resolved” by the interferometer. It is noteworthy that this happens at an order-of-magnitude similar separation as the resolution of two point sources by a filled aperture telescope; $s_{\text{binary}} = \lambda/B$ for a Rayleigh resolution criterion (cf. Jenkins and White 1957).

Even when the binary star is quasi-static, Equation 2.32 describes sinusoidal variations of the fringe visibility (squared modulus) with varying $\mathbf{B} \cdot \mathbf{s}_{\text{binary}}$; for ground based interferometers this variation occurs as a consequence of Earth rotation. Figure 2.7 depicts real \mathcal{V}^2 measurements on a binary star ι Pegasi, used to derive an orbit model for the system (Boden *et al.*, 1999).

2.8 Summary

In this Chapter we have discussed the response of interferometers to idealized astronomical sources. We have developed this theory in the context of typical detection strategies for optical interferometers: direct (*homodyne*) combination of the optical fields and detection by power-linear detectors. This is to be contrasted to the typical heterodyne, amplitude-linear

detection technologies used in radio interferometers (see Thompson, Moran, and Swenson 1986). Despite the technology differences between between radio and optical interferometers, a common characterization of source properties, namely the source visibility, suffices to give a qualitative and quantitative description of the interferometer response.

Visibility is a complex quantity whose amplitude (modulus) describes the intensity of the interferometric fringes, and whose phase describes the position of the fringes relative to a phase center. Sources that produce fringes (in the space of relative delay between the two interferometer arms) with an amplitude equal to the full received power of the source are said to have unit normalized visibility amplitude and are unresolved by the interferometer. Conversely, fringes with amplitudes less than the received power have normalized visibility amplitude less than one, and sources that produce such fringes are said to be resolved by the interferometer.

In ordinary circumstances the source visibility can be computed as a simple Fourier transform of the source brightness morphology, and an inverse Fourier transform of the source visibility function yields the source morphology. Techniques based on this relationship are given the term *synthesis imaging*, and have been employed for many years in radio interferometry (Perley *et al.*, 1989). Recently optical interferometers have begun making their first few forays into synthesis imaging (e.g. Baldwin *et al.* 1996). However, many optical interferometers today are limited to measurements of (squared) visibility amplitude, with no (useful) phase information available. Given our knowledge of expected source visibilities for different morphologies (e.g. uniform stellar disk, binary star), even such visibility amplitude measurements can be used to infer interesting properties of astronomical sources.

Acknowledgments

The work described in this manuscript was performed at the Infrared Processing and Analysis Center, California Institute of Technology, and the Jet Propulsion Laboratory under contract with the National Aeronautics and Space Administration. Thanks go to P.R. Lawson and M.M. Colavita for discussing various parts of the manuscript.

References

- J.E. Baldwin, M.G. Beckett, R.C. Boyesen, D. Burns, D.F. Buscher, G.C. Cox, C.A. Haniff, C.D. Mackay, N.S. Nightingale, J. Rogers, P.A.G. Sheuer, T.R. Scott, P.G. Tuthill, P.J. Warner, D.M.A. Wilson, and R.W. Wilson, “The first images from an optical aperture synthesis array: mapping of Capella with COAST at two epochs,” *Astron. Astrophys.* **306**, L13–L16 (1996).
- G.T. van Belle, B.F. Lane, R.R. Thompson, A.F. Boden, M.M. Colavita, P.J. Dumont, D.W. Mobjley, D. Palmer, M. Shao, G. Vasisht, J.K. Wallace, M.J. Creech-Eakman, C.D. Koresko, S.R. Kulkarni, X.P. Pan, and J. Gubler, “Radii and effective temperatures for G, K and M giants and supergiants,” *Astron. J.* **117**, 521–533 (1999).

- A.F. Boden, C.D. Koresko, G.T. van Belle, M.M. Colavita, P.J. Dumont, J. Gubler, S.R. Kulkarni, B.F. Lane, D. Mobley, M. Shao, and J.K. Wallace, “The visual orbit of Iota Pegasi,” *Astrophys. J.* **515**, 356–364 (1999).
- M. Born and E. Wolf, *Principles of Optics*, 7 (expanded) edn. (Cambridge, UK: Cambridge University Press, 1999).
- R. Hanbury Brown, J. Davis, and L.R. Allen, “The angular diameters of 32 stars,” *Mon. Not. R. Astron. Soc.* **167**, 121–136 (1974).
- A.R. Hajian, J.T. Armstrong, C.A. Hummel, J.A. Benson, D. Mozurkewich, T.A. Pauls, D.J. Hutter, N.M. Elias, K.J. Johnston, L.J. Rickard, and N.M. White, “Direct confirmation of stellar limb darkening with the Navy Prototype Optical Interferometer,” *Astrophys. J.* **496**, 484–489 (1998).
- D. Herbison-Evans, R. Hanbury Brown, J. Davis, and L.R. Allen, “A study of α Virginis with an intensity interferometer,” *Mon. Not. R. Astron. Soc.* **151**, 161–176 (1971).
- C.A. Hummel, J.T. Armstrong, D.F. Buscher, D. Mozurkewich, A. Quirrenbach, and M. Vivekanand, “Orbits of small angular scale binaries resolved with the Mark III Interferometer,” *Astron. J.* **110**, 376–390 (1995).
- C.A. Hummel, D. Mozurkewich, J.T. Armstrong, A.R. Hajian, N.M. Elias, and D.J. Hutter, “Navy Prototype Optical Interferometer observations of the double stars Mizar A and Matar,” *Astron. J.* **116**, 2536–2548 (1998).
- J.D. Jackson, *Classical Electrodynamics*, 3 edn. (New York: John Wiley and Sons, 1998).
- F. Jenkins and H. White, *Fundamentals of Optics* (New York: McGraw-Hill, 1957).
- A.A. Michelson, “On the application of interference methods to astronomical measurements,” *Phil. Mag.* **30**, 1–21 (1890).
- A.A. Michelson, “On the application of interference methods to astronomical measurements,” *Astrophys. J.* **51**, 257–262 (1920).
- A.A. Michelson and F.G. Pease, “Measurement of the diameter of α Orionis with the interferometer,” *Astrophys. J.* **53**, 249–259 (1921).
- D. Mozurkewich, K.J. Johnston, R.S. Simon, P.F. Bowers, R. Gaume, D.J. Hutter, M.M. Colavita, M. Shao, and X.P. Pan, “Angular diameter measurements of stars,” *Astron. J.* **101**, 2207–2219 (1991).
- R.A. Perley, F.R. Schwab, and A.H. Bridle, *Synthesis Imaging in Radio Astronomy* ASP Conf. Ser., **6** (Provo, UT: Brigham Young Univ. Press, 1989).
- A. Quirrenbach, D. Mozurkewich, D.F. Buscher, C.A. Hummel, and J.T. Armstrong, “Angular diameter and limb darkening of Arcturus,” *Astron. Astrophys.* **312**, 160–166 (1996).
- M. Shao, M.M. Colavita, B.E. Hines, J.L. Hershey, J.A. Hughes, D.J. Hutter, G.H. Kaplan, K.J. Johnston, D. Mozurkewich, R.S. Simon, and X.P. Pan, “Wide-angle astrometry with the Mark III interferometer,” *Astron. J.* **100**, 1701–1711 (1990).
- A.R. Thompson, J.M. Moran, and G.W. Swenson Jr., *Interferometry and Synthesis in Radio Astronomy* (New York: John Wiley and Sons, 1986).

